



Analysis of Wake Region Behind Bluff Body for Piezoelectric Energy Harvester

Open
Access

Mohd Nor Fakhzan Mohd Kazim^{1,*}, Rasidi Rasani², Mohd Zaki Nuawi², Zamri Harun², Yap Khang Hau¹, Mohd Shukry Abdul Majid¹

¹ School of Mechatronic Engineering, Universiti Malaysia Perlis (UniMAP), Pauh Putra Campus, 02600 Arau, Perlis, Malaysia

² Department of Mechanical and Materials Engineering, Faculty of Engineering and Built Environment, Universiti Kebangsaan Malaysia (UKM), 43600 UKM Bangi, Selangor, Malaysia

ARTICLE INFO

ABSTRACT

Article history:

Received 29 August 2018

Received in revised form 31 October 2018

Accepted 6 December 2018

Available online 18 March 2019

Inspired by enhancement of vortex induced vibration energy harvesting as a green and renewable energy source, several geometry shapes such as cylinder, square, triangle, D shape, and U shape bluff body were studied in terms of vortex shedding frequency, vorticity and pressure difference in order to determine the best bluff body for piezoelectric film. A 2-dimensional computational fluid dynamic (CFD) simulation analysis is carried out with the length and height of bluff body fixed as 0.1 m and air flow used for simulations are 0.0438 m/s, 0.292 m/s, and 0.73 m/s which corresponds to Reynolds number (Re) of 300, 2000, and 5000. Overall, cylinder, triangle, and D shape bluff body gives a higher vortex shedding frequency and Strouhal Number (St) compare to square and U shape. Triangle bluff body was able to maintain the highest vorticity for all three difference air speeds. It is found that maximum vorticity point will move backwards when higher air velocity is simulated. Nevertheless, triangle bluff body gave the highest-pressure difference reading among all tested shapes. In conclusion, triangle shape bluff body is the most suitable shape for inducing vortex shedding to piezoelectric film and it is suggested the length of the piezoelectric beam is between 0.05m and 0.15m.

Keywords:

Piezoelectric film, bluff body, wake region, vortex shedding frequency, vorticity, pressure difference.

Copyright © 2019 PENERBIT AKADEMIABARU - All rights reserved

1. Introduction

As consumption of electrical energy has been increasing year by year, mankind has built various large-scale power plants such as thermal, nuclear and hydro power plants to produce sufficient energy to fulfill our needs [1], [2]. However, these large-scale power plants usually cause tremendous damage to our nature environment due to excessive waste produced during construction of power plants and generation of electricity [3].

Due to the advancement of research and technology, scientists came up with materials such as piezoelectric element and solar cell which able to harvest energy from ambient environment so that

* Corresponding author.

E-mail address: fakhzan@unimap.edu.my (Mohd Nor Fakhzan Mohd Kazim)

it can generate energy without burning fuel or reconstructing the whole environment landscape. Therefore, harvesting ambient environmental energy is an effective alternative solution for sustainable energy [4].

Among all ambient energy existed, wind energy is regarded as one of the major renewable green energy [5]. The traditional way to harvest energy from wind is by building wind turbines which convert kinetic energy to electrical energy through the rotation of the wind blades and electromagnetic induction of turbines [6,7]. However, wind turbines are huge in size, complex, as well as costly.

Piezoelectric element can be considered as an alternative material that maybe utilized to harvest macro scale energy for devices and instruments through method such as Vortex Induced Vibration [8], and Wake Galloping [9]. From previous research [10-12], there were experimental and analysis regarding vortex-induced energy harvesting using piezoelectric cantilever in fluid.

There were different approaches in bluff body design used in previous experimental researches such as the classical cylindrical [13], rectangular [14], D shape [15], [16], triangle [17] and C shape [11]. Each of these designs have their own theories to enhance the effect of vortex and galloping effect. Therefore, in this paper comparisons will be made among these five bluff body designs and a suitable length of piezoelectric film will be deduced based on several analysis on vortex formation of each designs.

From previous research by B. Gandhi [18], it is proven that fluid flow towards different shapes of bluff body, Karman vortex street will form behind it with different drag, and lift coefficient. The formation of these vortices will cause changes in pressure behind the bluff body which is suitable to vibrate piezoelectric film. By making use of these vortices and uplifting forces, it can flutter piezoelectric film which are able to generate electricity. However, there are various types of bluff body designs that were experimented for different harvester application.

In terms of piezoelectric film, there are several types of dimensions. These dimensions will greatly affect the efficiency of energy harvesting system in terms of flexibility, fluttering amplitude as well as the frequency of vibration as mention by C. Lemaitre [19]. Moreover, changes in the dimension of the piezoelectric film will greatly affect the voltage output and fluttering condition. Hence, it is crucial to pick suitable dimension for the piezoelectric film in order to optimize the efficiency of the system.

This research is mainly focus on analyzing vortex shedding for each bluff body as well as choosing the suitable length for piezoelectric film that is suitable for specific bluff body under specific wind speed. However, the length of piezoelectric film is determined by analyzing velocity curl at 3 specific points downstream of the bluff body. This means that length proposed is based on behavior of fluid at downstream without piezoelectric film attached towards the bluff body.

2. Theoretical Background

Vortex shedding is based on theory of vortex formation that turbulent fluid flow will generate after passing over a structure when specific condition is applied, such as shape of structure and velocity of fluid flow. In other words, vortex shedding is an unstable condition where air flow over an obstacle will split into two separate streams and result in three flow instabilities which are boundary layer instability, separated shear layer instability, and Karman vortex instability.

2.1 Strouhal Number

Since vortex shed at the wake region of the body is in an alternating form, the vortex will appear periodically in Von Karman Vortex Street [20]. The frequency of this phenomenon can be represent

using Strouhal Number (St) which is shown in Eq. 1, where vortex shedding frequency (f), characteristic diameter of bluff body (D), and average velocity flow (μ) is used.

$$St = \frac{f \cdot D}{\mu} \quad (1)$$

In order to maximize the piezoelectric film vibration and conversion efficiency, the film is recommended to have the eigenfrequency that matches with vortex shedding frequency [21]. The matching frequency will resonate the fluctuation of piezoelectric film which is an advantage for the vortex induce vibration energy harvesting system.

2.2 Reynolds Number

Re is calculated based on the ratio of inertial forces of fluid to viscosity of fluid as in Eq. 2, where), average velocity flow (u), and kinematic viscosity of fluid (ν) is used.

$$Re = \frac{uD}{\nu} \quad (2)$$

When Re is high, it means that the inertial forces of the fluid will be the dominating factor that affect the overall condition of the fluid, resulting in turbulent flow.

2.3 Pressure Loss

The pressure loss is greatly affected by shape of obstacle, diameter ratio, and also viscosity of fluid. The turbulent flow in the wake is difficult to mathematically described with Navier–Stokes equation. Thus, the pressure difference ΔP can be estimated from Bernoulli's equation during laminar flow given in Eq. 3 where k is velocity ratio, v_{lam} is laminar velocity flow, and ρ is air flow density [21].

$$\Delta P = \frac{\rho}{2} \left(v_{lam}^2 - \left(v_{lam} - \frac{v_{lam}}{k} \right)^2 \right) \quad (3)$$

3. Modelling and Settings

The simulation is conducted under three different air flow velocity, 0.0438 m/s, 0.292 m/s, and 0.73 m/s which corresponds Re of 300, 2000, and 5000. In order to model all the three flows, three viscous models; laminar, transition SST 2 and standard k - ϵ with standard wall function, were used. In all three cases, standard air properties were used, where the fluid density $\rho = 1.185 \text{ kg/m}^3$ and the dynamic viscosity $\mu = 1.831 \times 10^{-5} \text{ kg/ms}$. The objective of this simulation is to obtain the optimum pressure point for each of the bluff body and compare which bluff body gives the pressure difference to vibrate the piezoelectric film.

3.1 Sketching

In Table 1 and Figure 1, the dimension of wind tunnel as well as bluff body is drawn and labelled. The length and diameter of bluff body were tuned to the same measurement in order to generate a fair test between each shape.

Table 1
 Dimension of bluff body

Bluff Body	$L \times D$
Cylinder	0.1 m x 0.1 m
Square	0.1 m x 0.1 m
Triangle	0.1 m x 0.1 m
U-Shape	0.1 m x 0.1 m
D-Shape	0.1 m x 0.1 m

The sketching for the design includes two components, which are air flow domain and cross section of bluff body. In this stage the dimensions of bluff body and air tunnel is fixed so that the data are standardized.

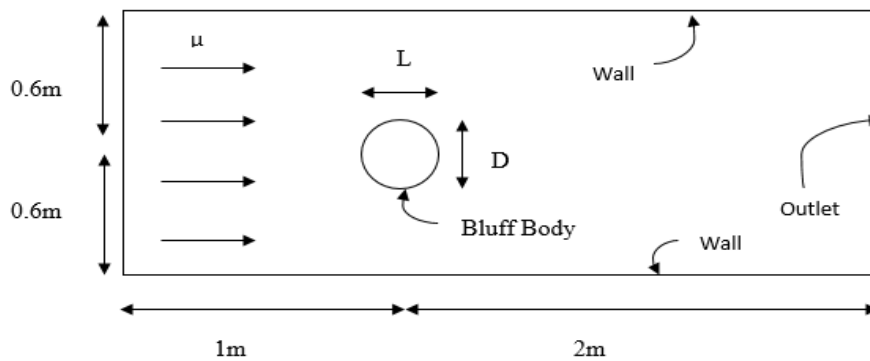


Fig. 1. Simulation setup wind direction towards model

3.2 Meshing

The meshing for the surface body is set to triangular mesh with max face size of 0.015m so that the overall mesh will be fine and even. While for the bluff body, it is set with edge sizing of 0.002m along with inflation or boundary layers by setting first layer thickness of 2.0×10^{-3} m with 20 layers and intra layer growth rate of 1.5. By doing so, the meshing around the bluff body will be evenly distributed according to the shape of the bluff body where the mesh skewness is around 0.63. The mesh result of cylinder is shown in Figure 2.

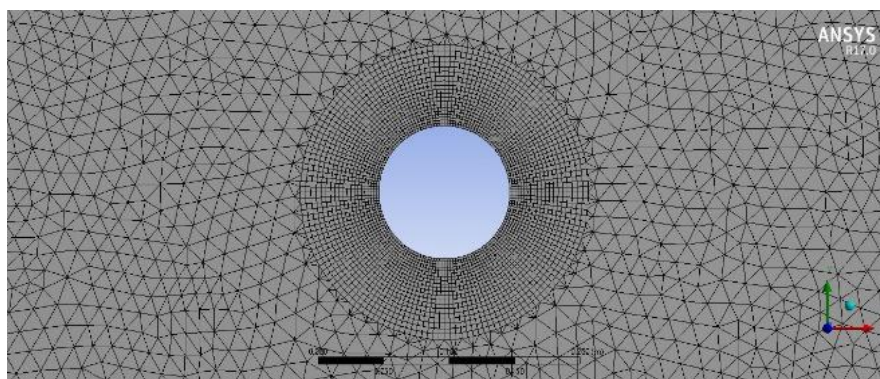


Fig. 2. Close-up view of meshing after inflation and edge sizing applied

As in Table 2, the nodes and elements in each design were listed after meshing process. This is to ensure the consistency and accuracy of the result

Table 2
 Number of nodes and elements after
 meshing process

Bluff Body	Nodes	Elements
Cylinder	20102	36368
Square	18563	34466
Triangle	18235	34582
U-Shape	18588	34579
D-Shape	19595	36110

3.3 Setting

All the settings that will be used for this simulation are tailored to three different Re categories. The three different categories of Re are 300, 2000, and 5000 which falls into laminar, transition, and turbulent categories respectively.

The solver that will be used in all the three categories of simulation will be set as pressure based, transient, with Semi-Implicit Method for Pressure-Linked Equations (SIMPLE) pressure-velocity coupling algorithm scheme. The detail settings that used for each of the models are listed in Table 3.

Table 3
 Settings for Different Types of Model

	Bluff Body	Nodes	Elements
	Least Squares Cell Based	Least Squares Cell Based	Least Squares Cell Based
	Gradient	Gradient	Gradient
	Second Order Pressure	Second Order Pressure	Second Order Pressure
	Second Order Upwind	Second Order Upwind	Second Order Upwind
	Momentum	Momentum	Momentum
Spatial Discretization		Second Order Upwind	Second Order Upwind
		Turbulent Kinetic Energy	Turbulent Kinetic Energy
		Second Order Upwind Specific	Second Order Upwind
		Dissipation Rate	Specific Dissipation Rate
		Second Order Upwind	
		Intermittency	
		Second Order Upwind	
		Momentum Thickness Re	
Transient Formulation	Second Order Implicit	Second Order Implicit	Second Order Upwind
Solution Initialization	Hybrid	Hybrid	Hybrid
Calculation Time	0.01s Time Step Size	0.01s Time Step Size	0.01s Time Step Size
Setting	2000 Number of Time Steps	2000 Number of Time Steps	2000 Number of Time Steps
	50 Max Iteration/Time Step	50 Max Iteration/Time Step	50 Max Iteration/Time Step
Turbulent Intensity	-	5%	5%
Turbulent Viscosity Ratio	-	10	10

The boundary condition of bluff body will be set as no slip condition while the fluid domain walls will be under free slip condition where air density and dynamic viscosity is 1.225 kg/m^3 and $1.7894 \times 10^{-5} \text{ kg/m}\cdot\text{s}$ respectively.

3.4 Post Processing

In order to obtain the optimum pressure difference downstream, three different points with a distance of 0.05 m, 0.15 m and 0.25 m are monitored to determine the maximum vorticity behind the bluff body as shown in Figure 3.

In order to get the specific values of pressure different for the highest vorticity point, two points will be created 0.025 m above and below from the highest vorticity point as shown in Figure 4.

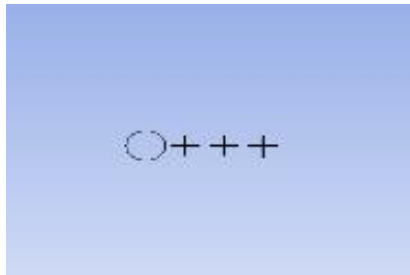


Fig. 3. Fixed points to determine maximum vorticity

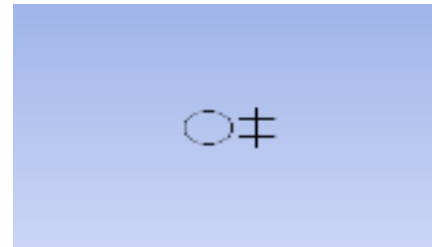


Fig. 4. Two points for pressure difference measurement

4. Results and Discussion

4.1 Grid Independent Study

The simulation research was undertaken after completing a grid independent study. This is to establish higher accuracy of the fluent simulation. The blunt body is analyzed using the laminar model with inlet velocity of 0.0438m/s. For the study, six different meshes applied to the model to predict the vortex strength in order to determine the optimal mesh quality for CFD simulation analysis. The grid independence study was established by varying the growth rate between 1.001 and 1.8 for the best computational accuracy with minimal computational time. From Figure 5, the vortex strength produces after the bluff body showed that the value increases from 0.31 s⁻¹ with 17486 elements to 4.0 s⁻¹ with 343844 elements for 0.05 m from the bluff body while for distance 0.15 m the vortex strength value increase from 0.4 s⁻¹ to 1.78 s⁻¹. The results obtained onward had a constant value around 1.8 which is an acceptable range. From the graph, the mesh above 3 x 10⁴ elements is adequate for the high computational accuracy.

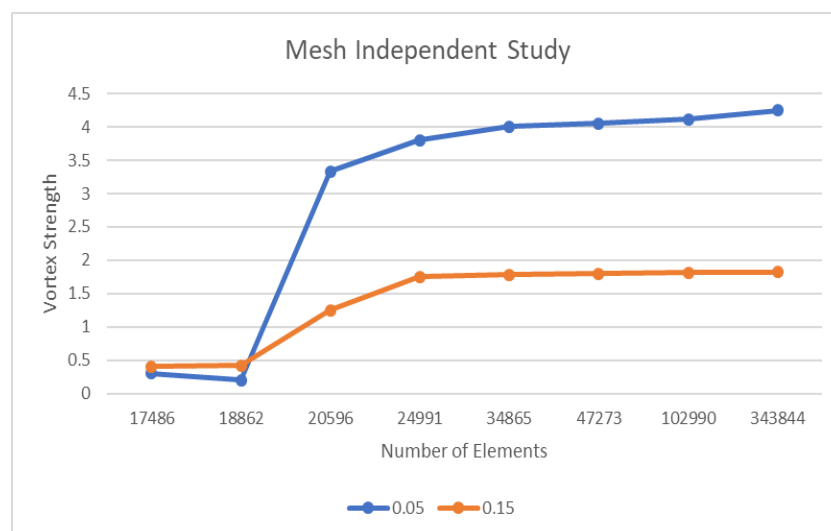


Fig. 5. Graph of the mesh independent study

4.2 Pressure Distribution

Figure 6 shows trend of St with increment of Re . Out of five shapes, two of them (square and U shape) have a same trend with a slight decrement from 0.17 to around 0.13. Cylinder and D shape shares the same pattern where it has the same St at Re 300 and decrease to 0.21 at transition Re , and increase back to 0.24 at Re 5000. On the other hand, triangle shape shows consistent trend for all Re .

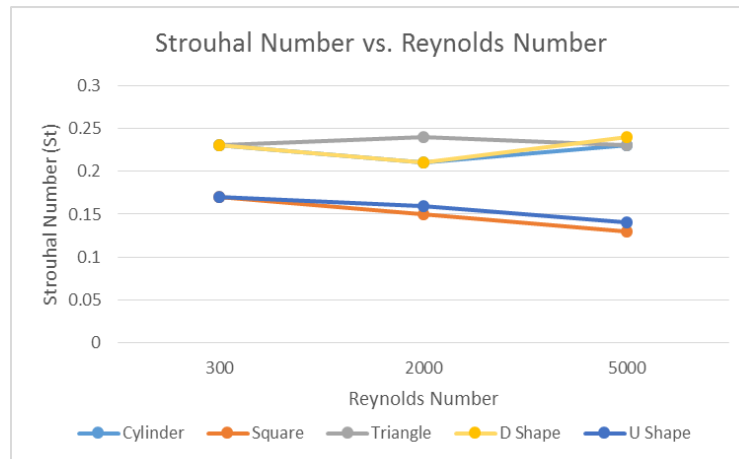


Fig. 6. Plot of St for each shape at different Re

However, there is an obvious difference in St for square and U-shape compare to the other shapes. This is due to the flat surface facing towards the air flow which causes flow separation to occurs on top and bottom face of square and U blunt body as shown in Figure 7 and Figure 8.

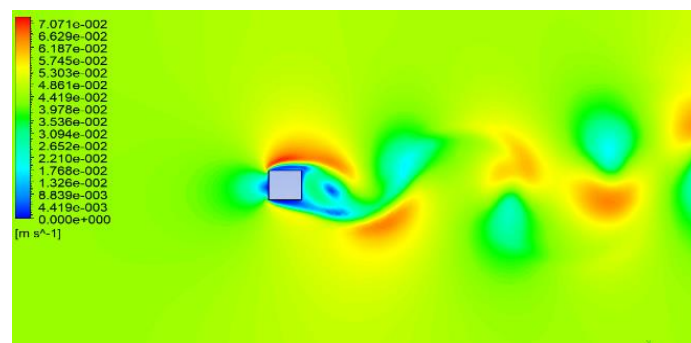


Fig. 7. Velocity Contour for Square bluff body at $Re = 300$

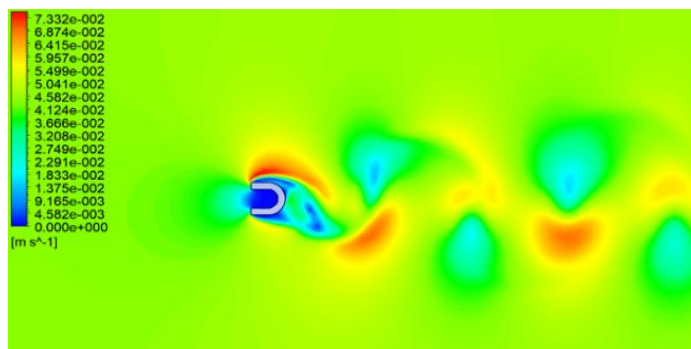


Fig. 8. Velocity Contour for U shape bluff body at $Re = 300$

From Figure 9, 10 and 11, cylinder, triangle and D shape bluff body are more favourable among the five bluff bodies in generating high vortex shedding frequency downstream, for the range of Re 300 to 5000, since the separation region is thinner than square and U shape bluff body.

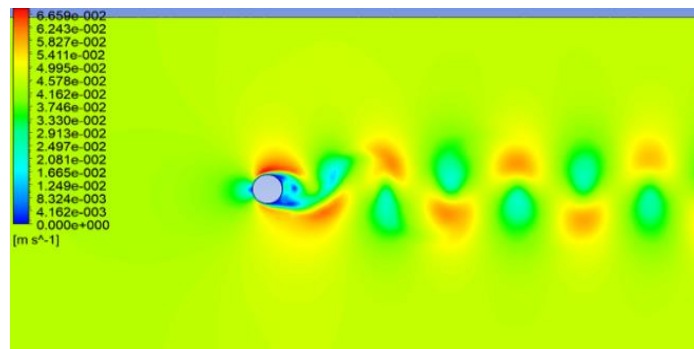


Fig. 9. Velocity Contour for Cylinder bluff body at Re = 300

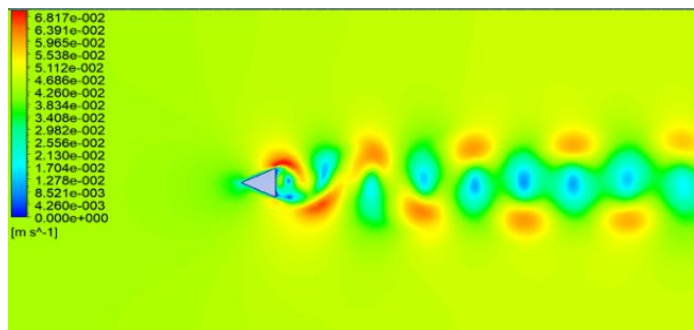


Fig. 10. Velocity Contour for Triangle bluff body at Re = 300

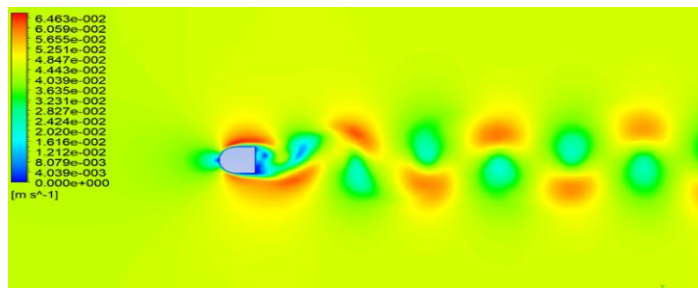


Fig. 11. Velocity Contour for D-shape bluff body at Re = 300

4.3 Vorticity at Re = 300

From the plot in Figure 11, it is obvious that all bluff bodies generate the highest vorticity at 0.05 m distance from the bluff body. Triangle and cylinder have a huge slump from 3.5 s^{-1} to 2 s^{-1} and 2.3 s^{-1} to 1.2 s^{-1} respectively when distance increases from 0.05 m to 0.15 m. Meanwhile, for square, D, and U shape show a steady decrement when the distance is increased by 0.1 m. It is clear, when the distance is increased to 0.25 m all the shapes have slight decrease in vorticity. The graph in Figure 12 shows that triangle bluff body gave the highest vorticity among all the shapes at Re = 300 and is expected to produce the highest-pressure difference according to this set of data.

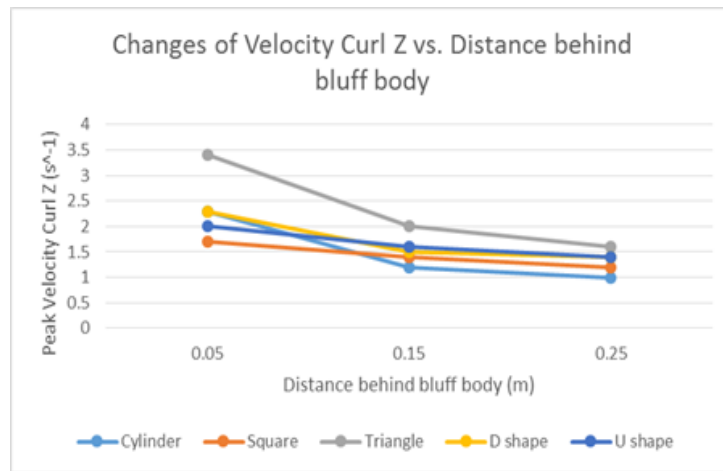


Fig. 12. Changes of velocity curl z at Re = 300

4.4 Vorticity at Re = 2000

From Figure 13, triangle generates the highest vorticity of 32 s^{-1} followed by cylinder and U shape with value of 22 s^{-1} and 16 s^{-1} respectively. Subsequently, these three shapes have the same pattern where there is a huge decline of vorticity from 0.05 m to 0.15 m. Besides that, D and square shape bluff body have the lowest starting velocity of 1.9 s^{-1} and 6 s^{-1} at 0.05 m point. However, D and square shape show vorticity increase when the distance is increased by 0.1m. Finally, at 0.25 m point, all shapes have vorticity which falls between 5 s^{-1} and 10 s^{-1} . Although the vorticity for all bluff bodies fall in the range between 5 s^{-1} to 10 s^{-1} , triangle gives the highest vorticity value among all which is 10 s^{-1} .

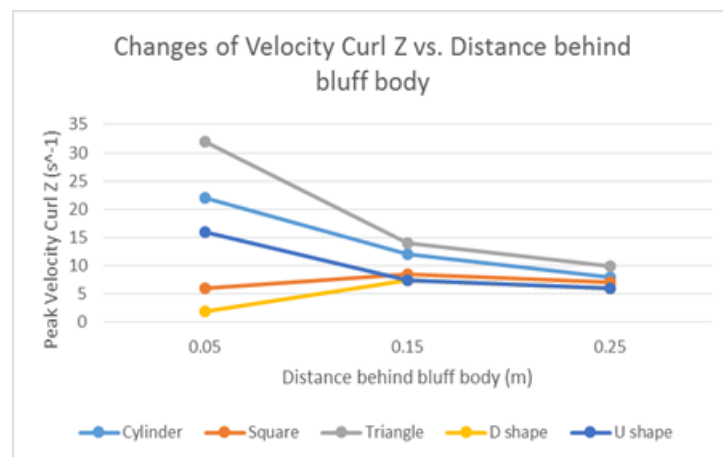


Fig. 13. Changes of velocity curl z at Re = 2000

4.5 Vorticity at Re = 5000

According to Figure 14, the vorticity for triangle bluff body drastically decreases from 34 s^{-1} to 20 s^{-1} between 0.05 m and 0.15 m. Square and U shape bluff body shows increasing trend from 0.05 m to 0.25 m in terms of vorticity value (i.e 1 s^{-1} to 8 s^{-1} and 3 s^{-1} to 13 s^{-1} respectively). D shape and cylinder bluff body, shows the best vorticity value of 20 s^{-1} and 15 s^{-1} respectively at 0.15 m point. Although the maximum vorticity point has changed according to increment in wind speed, triangle bluff body still perform well at 0.05 m point which gives the highest vorticity value among all other bluff bodies.

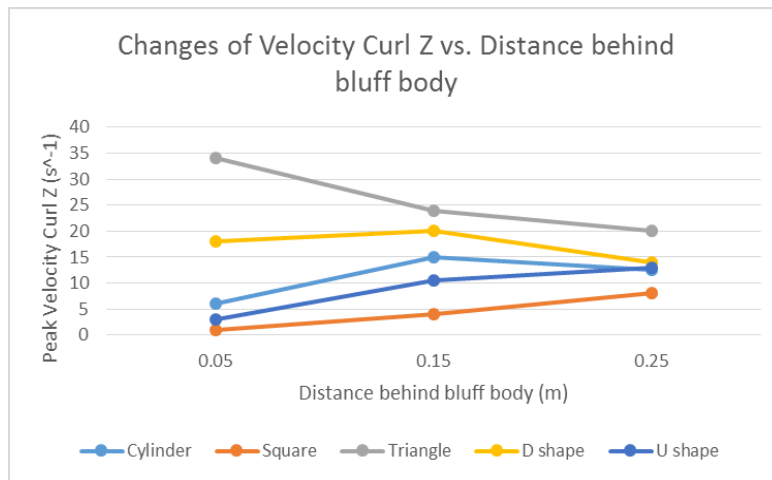


Fig. 14. Changes of velocity curl z at Re = 5000

By comparing Figure 15, 16 and 17 it can be seen that there is a huge low velocity region right behind square and U shape bluff body compared to the cylinder bluff body. This can explain the higher vorticity of cylinder compared to square and U shape at 0.05 m point.

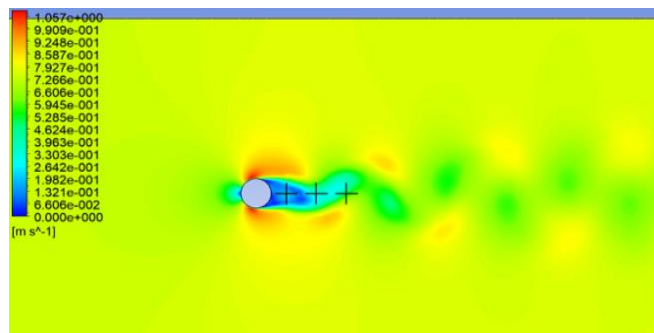


Fig. 15. Velocity contour for cylinder at Re = 5000

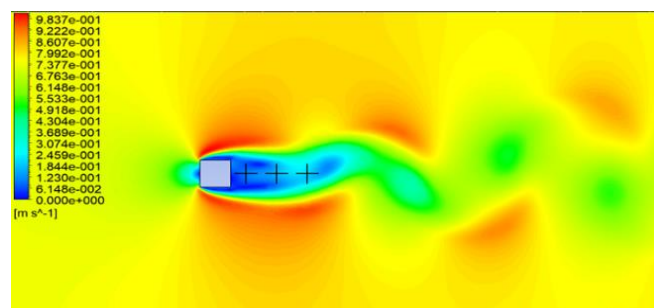


Fig. 16. Velocity contour for square at Re = 5000

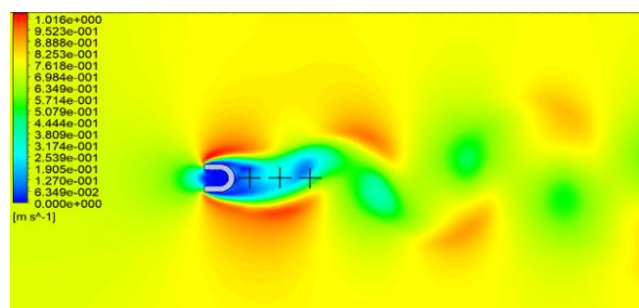


Fig. 17. Velocity contour for U shape at Re = 5000

On the other hand, Figure 18 and Figure 19 shows the velocity profile of triangle and D shape have a much smaller low velocity region right behind the bluff body compared to the three other shapes. However, triangle gives the highest vorticity among all.

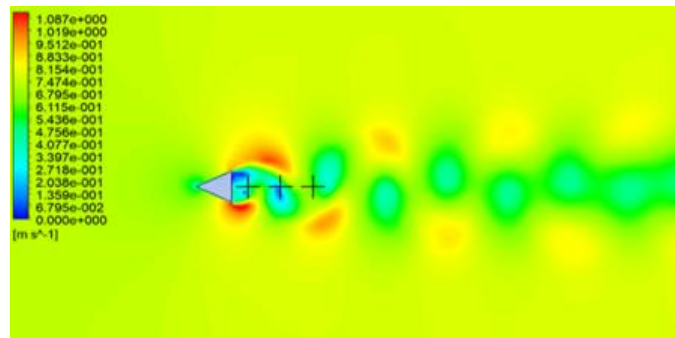


Fig. 18. Velocity contour for Triangle shape at Re = 5000

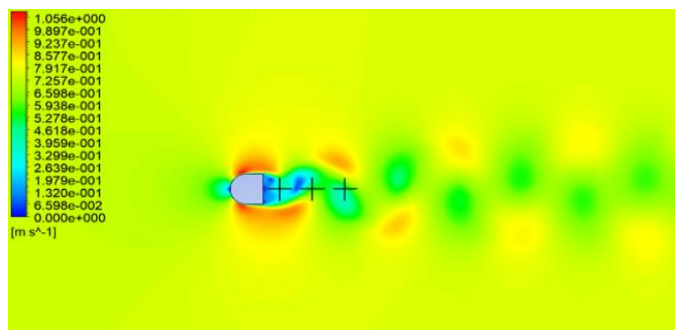


Fig. 19. Velocity contour for D shape at Re = 5000

4.6 Pressure Difference

Fluctuating a piezoelectric film attached downstream of a bluff body needs a pressure difference that provide force towards the film in d_{31} direction. Since the bluff body is placed under windy condition, vortex will be the main force provider which cause pressure difference on the surface of the piezoelectric film.

As shown from the graph in Figure 20, triangle is able to generate the highest-pressure difference which is 2.25×10^{-3} Pa at Re = 300. The second highest pressure difference is given by D shape with 1.50×10^{-3} Pa. However, cylinder, square and U shape are able to produce around 1.00×10^{-3} Pa pressure difference which is 1.25×10^{-3} Pa less than triangle.

The secondary vortex induced peak mentioned by Q. Wen *et al.*, [18], had appeared in all bluff body but the effect is less for triangle and D shape as shown in Figure 21. The effect of secondary vortex induced peak which are bounded with rectangle and circle in Figure 21 will cause an extra damping towards piezoelectric film and the efficiency of energy harvester will be greatly reduced by it.

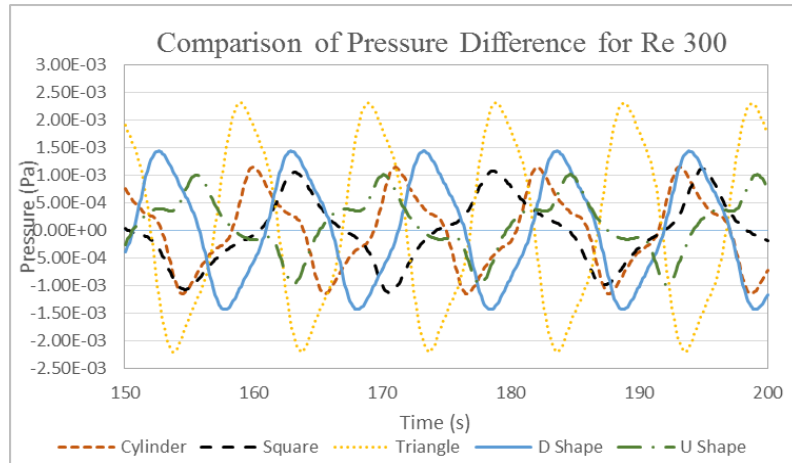
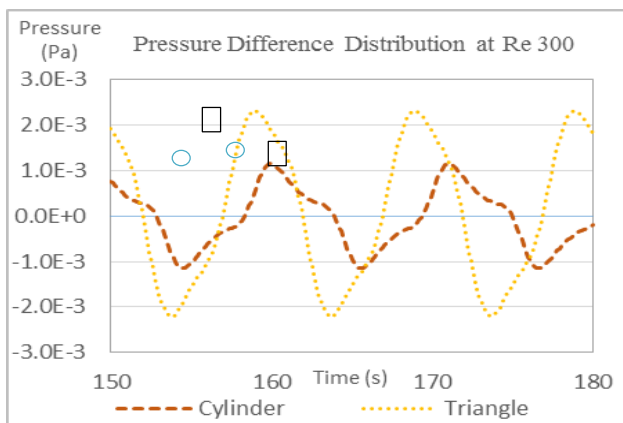
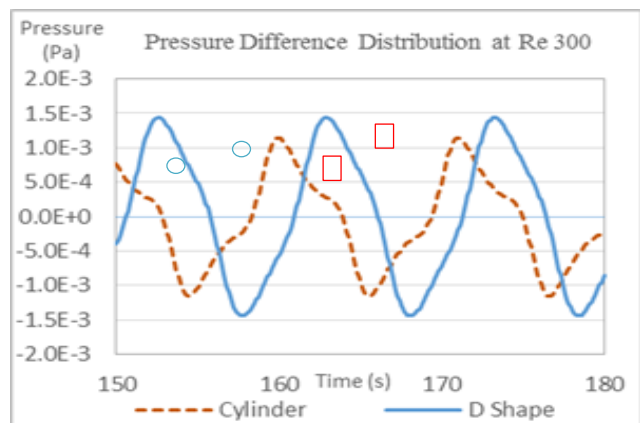


Fig. 20. Comparison of pressure difference for each bluff bodies at Re = 300



(a) Cylinder to Triangle



(b) Cylinder to D shape

Fig. 21. Comparison of secondary vortex induced peak for at Re = 300

For Re = 2000 pressure difference, triangle bluff body shows the highest-pressure difference of 0.15 Pa. It is 0.1275 Pa higher than pressure generated by D shape as shown in Figure 22. For Re = 2000, U shape gives the least pressure difference which is around 1.25×10^{-3} Pa. In contrast, triangle have a pressure peak difference of around 0.1488 Pa.

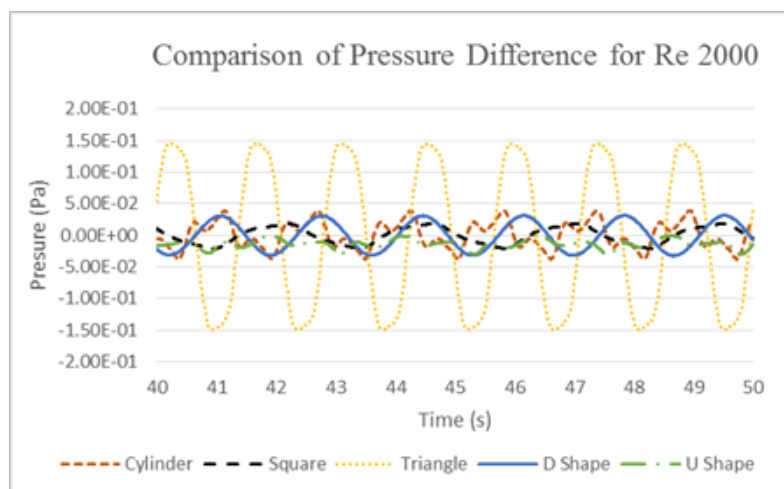


Fig. 22. Comparison of pressure difference for each bluff bodies at Re = 2000

The secondary vortex induced peak effect is less obvious for triangle and D shape bluff body compared to $Re = 300$. It appears that D shape have none of the secondary induced peak effect or in other words D shape have a perfect sinusoidal wave for $Re = 2000$.

According to the graph in Figure 23, triangle gives the best generated pressure difference among all shapes which is 0.6 Pa. For the other four shapes the pressure difference was maintained around 0.25 Pa. By comparing shapes to other, triangle bluff body has a 140% larger pressure.

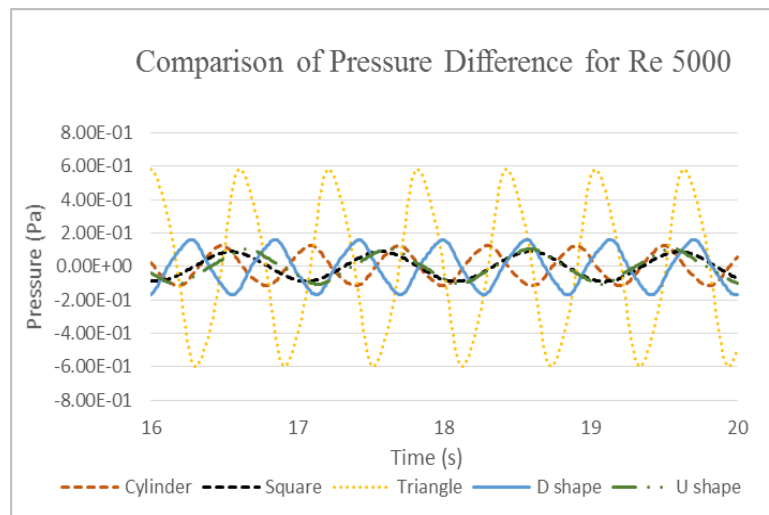


Fig. 23. Comparison of pressure difference for each bluff bodies at $Re = 5000$

Overall, triangle bluff body is shown to be the best bluff body in generating high pressure difference at the downstream. The simulation result from Figure 20, 21 and 22 have shown triangle as a consistent bluff body that able to generate high pressure difference and less effected by secondary vortex.

5. Conclusions

From this project, five different shapes of bluff body that were widely used by previous researcher were picked and compared for three different air velocity; 4.38×10^{-2} m/s, 0.292 m/s, and 0.73 m/s.

For St , three shapes; cylinder, triangle, and D, gives the best results compared to square and U shape. The increase of flow separation is due to flat surface against the air flow. By comparing St against Re , the result for triangle bluff body showed St was maintained around 0.23 for Re 300 to 5000. For square and U shape, the trend of St decreases from 0.17 to 0.13 when Re increases. However, for D shape and cylinder, both experienced a slight decrement of St from 0.23 to 0.21 from $Re = 300$ to 2000.

The maximum vorticity point for each bluff body differs when Re increases. From simulation, the result for triangle is the most consistent among all which gives the best value at 0.05m even while Re increases from 300 to 5000. Subjectively, it is also found that the vortices formation for cylinder, square and U shape moves backwards as Re increases. Thus, the separation distance of 0.05m is the best place to pivot piezoelectric flag.

As for pressure difference, triangle bluff body poses the best shape in generating high pressure difference downstream of the bluff body. The pressure difference obtained from triangle shape is 2.25×10^{-3} Pa, 0.15 Pa, and 0.6 Pa for $Re = 300$, 2000 and 5000 respectively. It is found that at $Re =$

5000, the effect secondary vortex induced peak is less obvious compare to lower Re. D-shape took the second-best shape in generating high pressure difference of 1.50×10^{-3} Pa, 2.25×10^{-2} Pa, and 0.15 Pa when Re increase from 300 to 5000. Triangle and D shape also showed reduced effect on secondary vortex induced peak.

Finally, triangle is the most suitable, followed by D shape for piezoelectric film where all the criteria that were needed for piezoelectric film fluctuation was met. As for length of piezoelectric film, it is recommended to place film between 0.05m and 0.15m after the bluff body. The proposed position is in accordance to $L = 2.25D$ in [14] which will eliminate possibility of second vibration mode.

Acknowledgements

This research was finance by the Ministry of Education (MOE) Malaysia via the Fundamental Research Grant Scheme; Ref: FTGS-MRSA/1/2018/TK05/UNIMAP/01/1). The author would like to acknowledge Universiti Malaysia Perlis (UniMAP) for laboratory and technical assistance.

References

- [1] U.S. Energy Information Administration, International Energy Outlook. (2017): 42
- [2] Khattak, Muhammad Adil, Mohammad Azfar Haziq Ayoub, Muhammad Ariff Fadhilillah Abdul, Mohd Faidhi Mahrul Manaf, Mohd Ridwan Mohd Juhari, Mira Idora Mustafa, and Suhail Kazi "Global Energy Security and European Union: A Review," *Journal of Advanced Research in Applied Sciences and Engineering Technology* 11, no. 1 (2018): 64–81
- [3] "TOTAL FAILURE of the climate crusade": Coal power has the same energy share it had 20 years ago.
- [4] Penella, M. T., and M. Gasulla. "A review of commercial energy harvesters for autonomous sensors." In *2007 IEEE instrumentation & measurement technology conference IMTC 2007*, pp. 1-5. IEEE, 2007.
- [5] Herbert, GM Joselin, Selvaraj Iniyan, E. Sreevalsan, and S. Rajapandian. "A review of wind energy technologies." *Renewable and sustainable energy Reviews* 11, no. 6 (2007): 1117-1145.
- [6] "How Is Electricity Generated - Electrical Energy Production." [Online]. Available: <https://www.electricityforum.com/how-is-electricity-generated>. [Accessed: 26-Apr-2018].
- [7] A. M. S. Zuan, M. K. Z. Anuar, S. Syahrullail, M. N. Musa, and E. A. Rahim, "A Study of Float Wave Energy Converter (FWEC) Model," *Journal of Advanced Research in Applied Sciences and Engineering Technology* 1, no. 1 (2015):10
- [8] Caliò, Renato, Udaya Rongala, Domenico Camboni, Mario Milazzo, Cesare Stefanini, Gianluca De Petris, and Calogero Oddo. "Piezoelectric energy harvesting solutions." *Sensors* 14, no. 3 (2014): 4755-4790.
- [9] Abdelkefi, A., J. M. Scanlon, E. McDowell, and Muhammad R. Hajj. "Performance enhancement of piezoelectric energy harvesters from wake galloping." *Applied Physics Letters* 103, no. 3 (2013): 033903.
- [10] Song, Rujun, Xiaobiao Shan, Fengchi Lv, and Tao Xie. "A study of vortex-induced energy harvesting from water using PZT piezoelectric cantilever with cylindrical extension." *Ceramics International* 41 (2015): S768-S773.
- [11] El-Mageed, Mostafa G. Abd, Mustafa Arafa, and Mohamed Elaraby. "Simulation and experimental investigation of an energy harvester utilizing flow-induced vibration." In *ASME 2014 International Design Engineering Technical Conferences and Computers and Information in Engineering Conference*, pp. V008T11A089-V008T11A089. American Society of Mechanical Engineers, 2014.
- [12] Gao, Xiu, Zhike Xu, Juping Gu, Feifei Pan, and Xiaoxiao Dong. "A study of piezoelectric generator based on the flow around a blunt body." In *2014 17th International Conference on Electrical Machines and Systems (ICEMS)*, pp. 2877-2881. IEEE, 2014.
- [13] Akaydin, H. D., N. Elvin, and Y. Andreopoulos. "The performance of a self-excited fluidic energy harvester." *Smart materials and Structures* 21, no. 2 (2012): 025007.
- [14] Taylor, George W., Joseph R. Burns, S. A. Kammann, William B. Powers, and Thomas R. Welsh. "The energy harvesting eel: a small subsurface ocean/river power generator." *IEEE journal of oceanic engineering* 26, no. 4 (2001): 539-547.
- [15] Pobering, S., S. Ebermeyer, and N. Schwesinger. "Generation of electrical energy using short piezoelectric cantilevers in flowing media." In *Active and Passive Smart Structures and Integrated Systems 2009*, vol. 7288, p. 728807. International Society for Optics and Photonics, 2009.
- [16] Qureshi, Fassahat Ullah, Ali Muhtaroglu, and Kağan Tuncay. "Near-optimal design of scalable energy harvester for underwater pipeline monitoring applications with consideration of impact to pipeline performance." *IEEE Sensors Journal* 17, no. 7 (2017): 1981-1991.

-
- [17] Sirohi, Jayant, and Rohan Mahadik. "Piezoelectric wind energy harvester for low-power sensors." *Journal of Intelligent Material Systems and Structures* 22, no. 18 (2011): 2215-2228.
- [18] Gandhia, B. K., S. N. Singh, V. Seshadri, and Jeot Singh. "Effect of bluff body shape on vortex flow meter performance." (2004).
- [19] Lemaitre, C., Pascal Hémon, and Emmanuel De Langre. "Instability of a long ribbon hanging in axial air flow." *Journal of Fluids and Structures* 20, no. 7 (2005): 913-925.
- [20] Haque, Rejaul, and M. Chowdhury. "Numerical study of vortex induced vibration of various bluff bodies for design optimization of a energy harvester." *Journal of Emerging Trends in Engineering and Applied Sciences* 6, no. 2 (2015): 144-150.
- [21] Wen, Quan, Robert Schulze, Detlef Billep, Thomas Otto, and Thomas Gessner. "Modeling and Optimization of a Vortex Induced Vibration Fluid Kinetic Energy Harvester." *Procedia Engineering* 87 (2014): 779-782.